

Reducing the dimensionality of grid based methods for electron-atom scattering calculations below ionization threshold



Jakub Benda*, Karel Houfek

Institute of Theoretical Physics, Charles University in Prague, V Holešovičkách 2, Prague, Czech Republic

ARTICLE INFO

Article history:

Received 17 September 2016
 Received in revised form 29 November 2016
 Accepted 3 December 2016
 Available online 10 December 2016

Keywords:

Electron-hydrogen scattering
 Exterior complex scaling
 B-splines

ABSTRACT

For total energies below the ionization threshold it is possible to dramatically reduce the computational burden of the solution of the electron-atom scattering problem based on grid methods combined with the exterior complex scaling. As in the R -matrix method, the problem can be split into the inner and outer problem, where the outer problem considers only the energetically accessible asymptotic channels. The $(N + 1)$ -electron inner problem is coupled to the one-electron outer problems for every channel, resulting in a matrix that scales only linearly with size of the outer grid.

© 2016 Elsevier B.V. All rights reserved.

1. Introduction

The quantum collisions of electrons with atoms belong today among classical disciplines of the quantum physics. Throughout the decades several successful calculation methods emerged, which are able to simulate the collisions to a good accuracy. A few notable examples are the R -matrix method [1], the convergent close coupling [2,3] and various formulations of direct discretization of the Schrödinger equation, like the finite element discrete variable representation with exterior complex scaling [4] and other grid based methods.

The exterior complex scaling (ECS) method has been popularized in quantum electron-atom scattering calculations by McCurdy and Rescigno [5] as a simple tool to replace outgoing-wave boundary conditions by Dirichlet boundary conditions when numerically solving the scattering Schrödinger equation discretized using the finite difference or finite element approach or using a B-spline basis. Bartlett [6] developed a modification for electron-hydrogen scattering (and other two-dimensional systems) – the “Propagating ECS” – where the sparse two-dimensional problem is reformulated as a sequence of dense one-dimensional problems. Volkov et al. [7] suggested further extension of ECS for scattering on charged ions employing the potential splitting approach. There is also a freely available implementation of the ECS method for electron-hydrogen scattering in the B-spline radial basis [8] based on the work of McCurdy and Martín [9].

While ECS has been particularly useful above the ionization threshold, where the proper boundary condition is complicated,

the usage of ECS below the ionization threshold is possible, too, without any modification. However, close above the excitation thresholds it is necessary to account for the long-range dipole (and higher multipole) coupling, see [10], by extending the simulated domain to large radii: to thousands of atomic units, or even more. This can be to some degree circumvented by radial extrapolation of the calculated cross sections as suggested by Bartlett [11]. In dense environment the inter-particle Coulomb potentials are effectively damped and need not be considered to so large distances, see [12]. Generally, in an N -electron atom the scattering wave-function for a fixed angular state is $(N + 1)$ -dimensional, hence its size – and likewise the rank of the matrix of the system that is to be solved in a particular basis – rises with the domain size to the $(N + 1)$ th power.

In further text a one-electron atom is assumed, as the main purpose of this extension is to speed up the implementation [8]. It is, nevertheless, very straightforward to generalize the theory to many-electron atoms and other multidimensional scattering systems.

The discussion deals only with total energies below the ionization threshold. The reason for this is that the proposed method expands parts of the solution as a linear combination of energetically allowed bound states. This is not advantageous close to and above the ionization threshold, because the number of allowed channels considerably increases. But sufficiently below the ionization threshold there are only a handful of bound states and the new approach then allows more efficient application of the chosen grid based method. It is then possible to accurately simulate the scattering at low impact energies even on excited targets, where the above mentioned long-range effects are more pronounced.

* Corresponding author.

E-mail address: jakub.benda@seznam.cz (J. Benda).

In practical calculations the grid can always support only a finite number of bound states and just a discrete subset of the continuum states, so the *a priori* restriction on below-ionization energies due to an unbounded amount of states is more or less artificial. Instead of the eigenstates given by analytic expressions one could employ bound states and a discretization of the continuum obtained by some numerical approach, for example, using the Sturmian basis. This is a straightforward generalization of the present method, which allows its extension to above-ionization energies. For clarity, though, we restrict the further presentation only to the exact bound states and low energies.

2. Theory

In the case of the scattering of an electron on a hydrogen atom the complete wave function for a fixed total spin S can be written as

$$\Psi^S(\mathbf{r}_1, \mathbf{r}_2) = \Psi_i^S(\mathbf{r}_1, \mathbf{r}_2) + \Psi_{sc}^S(\mathbf{r}_1, \mathbf{r}_2) \quad (1)$$

$$= \psi_{n_i l_i m_i}(\mathbf{r}_1) e^{i\mathbf{k}_i \cdot \mathbf{r}_2} + \frac{1}{r_1 r_2} \sum_{LM \ell_1 \ell_2} \psi_{sc, \ell_1 \ell_2}^{LMS}(r_1, r_2) \mathcal{Y}_{\ell_1 \ell_2}^{LM}(\hat{\mathbf{r}}_1, \hat{\mathbf{r}}_2) \quad (2)$$

and the Schrödinger equation as

$$(E_{tot} - H_{full}) \Psi_{sc}^S = H_{int} \Psi_i^S, \quad (3)$$

where the following property of the initial state has been used:

$$(E_{tot} - H_{free}) \Psi_i^S = 0, \quad (4)$$

with $H_{full} = H_{free} + H_{int}$. The free and interaction hamiltonians are

$$H_{free} = -\frac{\nabla_1^2}{2} - \frac{\nabla_2^2}{2} - \frac{1}{r_1}, \quad (5)$$

$$H_{int} = \frac{1}{r_{12}} - \frac{1}{r_2}, \quad (6)$$

where indices 1 are related to the atomic electron and indices 2 to the projectile electron. The right-hand side of (3) is symmetrized or antisymmetrized prior to the solution, depending on the value of S . The set of equations for the individual components $\psi_{sc, \ell_1 \ell_2}^{LMS}$ of the angular expansion in (1) can be obtained by a projection of Eq. (3) on the coupled angular state $\mathcal{Y}_{\ell_1 \ell_2}^{LM}$ resulting in

$$\sum_{\ell'_1 \ell'_2} \left[(E_{tot} - H_1 - H_2) \delta_{\ell'_1 \ell'_2}^{\ell_1 \ell_2} - V_{12} \right] \psi_{sc, \ell'_1 \ell'_2}^{LMS} = \chi_{\ell_1 \ell_2}^{LMS}, \quad (7)$$

where the electron–electron interaction potential V_{12} is given by

$$V_{12} = \sum_{\lambda} f_{\ell_1 \ell_2 \ell'_1 \ell'_2; L}^{\lambda} \frac{r_{<}^{\lambda}}{r_{>}^{\lambda+1}} \quad (8)$$

and the angular integrals $f_{\ell_1 \ell_2 \ell'_1 \ell'_2; L}^{\lambda}$ are defined in Eq. (6.41) of [13].

A typical visualization of the radial part of the solution is presented in Fig. 1, where it is apparent that apart from the evanescent waves running along the axes, in most of the coordinate space the wave function is equal to zero.

An arbitrary two-dimensional wave-function can be expanded into a complete basis of hydrogen eigenstates $P_{n\ell}$ in either of its coordinates,

$$\psi_{sc, \ell_1 \ell_2}^{LMS}(r_1, r_2) = \sum_m F_{m\ell_1}^{(1)}(r_1) P_{m\ell_2}(r_2) = \sum_n P_{n\ell_1}(r_1) F_{n\ell_2}^{(2)}(r_2).$$

The sum-integral symbol represents a summation over bound states and an integration over the continuous part of the spectrum, though in the numerical realization on a grid there are discrete states only. The expansion is valid for all coordinates r_1 and r_2 .

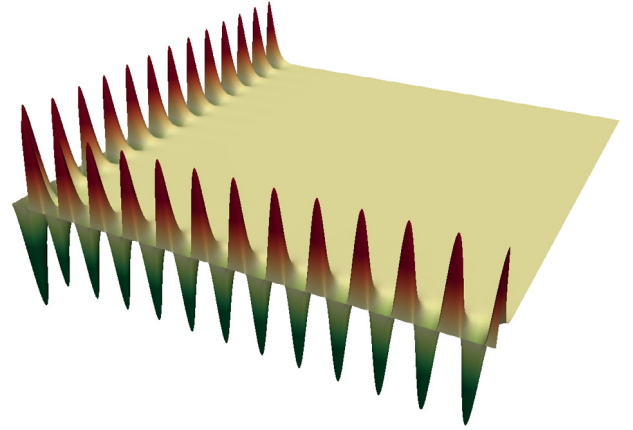


Fig. 1. Angular segment $\psi_{sc,00}^{000}$ of the scattering wave function at total energy $E_{tot} = -0.35$ Ry for initial state $H(1s)$. Cropped at $r_{1,2} = 100$ a.u.

However, if one of the coordinates is large enough, the expansion can be simplified, because the channel functions F_n corresponding to energetically forbidden channels exponentially vanish. In asymptotic distances, where $r_2 \ll r_1 \rightarrow +\infty$ or $r_2 \ll r_1 \rightarrow +\infty$, the electrons become distinguishable and the atomic electron, which is bound to the nucleus, has to be in one of the energetically allowed atomic states. It is then

$$\psi_{sc, \ell_1 \ell_2}^{LMS}(r_1, r_2) \rightarrow \begin{cases} \sum_{m=1}^{N_c^{(1)}} F_{m\ell_1}^{(1)}(r_1) P_{m\ell_2}(r_2) & [r_1 \rightarrow +\infty], \\ \sum_{n=1}^{N_c^{(2)}} P_{n\ell_1}(r_1) F_{n\ell_2}^{(2)}(r_2) & [r_2 \rightarrow +\infty], \\ 0 & [r_1, r_2 \rightarrow +\infty], \end{cases} \quad (9)$$

where $P_{n\ell}(r) = rR_{n\ell}(r)$ is the hydrogen bound state radial function multiplied by the radius, $F_{n\ell}^{(a)}(r)$ is the corresponding (unknown) projectile channel function for asymptotic $r_a \rightarrow +\infty$ and $N_c^{(a)}$ is the number of possible scattering channels. The summation over m and n includes only energetically allowed states, i.e. states with energy lower than the total energy E_{tot} . Note that the channel functions $F_{n\ell}^{(a)}$ should actually bear all the indices of $\psi_{sc, \ell_1 \ell_2}^{LMS}$, because they are unique for each of these angular components. However, most of the discussion deals with a single block for given angular momenta, so we use a simplified notation without these indices.

The asymptotic forms (9) can be plugged into the scattering equation (7), resulting in (for $r_1 \rightarrow +\infty$)

$$[(E_{tot} - E_m^{at}) - T_{\ell_1}] F_{n\ell_1}^{(1)} = \xi_{n\ell_2}^{(1)} + \sum_{\substack{\ell'_1 \ell'_2 m \\ \lambda > 0}} f_{\ell_1 \ell_2 \ell'_1 \ell'_2; L}^{\lambda} \frac{\rho_{n\ell_2, m\ell'_2}^{\lambda}}{r^{\lambda+1}} F_{m\ell'_1}^{(1)}, \quad (10)$$

where

$$\xi_{n\ell_2}^{(1)}(r_1) = \int P_{n\ell_2}(r_2) \chi_{\ell_1 \ell_2}^{LMS}(r_1, r_2) dr_2 \quad (11)$$

and

$$\rho_{n\ell_2, m\ell'_2}^{\lambda} = \int P_{n\ell_2}(r_2) r_2^{\lambda} P_{m\ell'_2}(r_2) dr_2, \quad (12)$$

or similarly

$$[(E_{tot} - E_n^{at}) - T_{\ell_2}] F_{m\ell_2}^{(2)} = \xi_{m\ell_1}^{(2)} + \sum_{\substack{\ell'_1 \ell'_2 n \\ \lambda > 0}} f_{\ell_1 \ell_2 \ell'_1 \ell'_2; L}^{\lambda} \frac{\rho_{m\ell_1, n\ell'_1}^{\lambda}}{r^{\lambda+1}} F_{n\ell'_2}^{(2)} \quad (13)$$

for the other asymptote ($r_2 \rightarrow +\infty$). The kinetic energy operators are

$$T_{\ell_i} = -\frac{1}{2} \frac{\partial^2}{\partial x_i^2} + \frac{\ell_i(\ell_i + 1)}{2r_i^2}.$$

The proposition (9) is satisfied very accurately already for moderate distances, because all energetically forbidden channels F_n exponentially decrease with the distance and only the asymptotically allowed states P_{nl} remain in the expansion. If there is a distance R_a where (9) is satisfactorily accurate, it is possible to solve the problem (7) only for radii smaller than R_a and Eqs. (10) and (13) only beyond the dividing radius R_a . The only remaining question is that of the boundary conditions, for which we will use ECS, and of the continuity, which is discussed further in the B-spline framework.

$$\psi_{sc,\ell_1\ell_2}^{LMS}(r_1, r_2) = \sum_{k,l=1}^N B_k(r_1)B_l(r_2)\psi_{sc,\ell_1\ell_2,kl}^{LMS}, \quad (14)$$

$$F_{m\ell_1}^{(1)}(r_1) = \sum_{k=1}^N B_k(r_1)F_{m\ell_1,k}^{(1)}, \quad (15)$$

$$F_{n\ell_2}^{(2)}(r_2) = \sum_{l=1}^N B_l(r_2)F_{n\ell_2,l}^{(2)}. \quad (16)$$

The B-splines are hill-like polynomial functions with given order O and compact support [14]. They are defined by a knot sequence; each B-spline then spans $O + 1$ knots. Likewise, only $O + 1$ B-splines contribute to the point value of a function they approximate. Every B-spline in a basis overlaps with $2O$ other B-splines. The full problem knot sequence is chosen along an ECS contour (as in [8]), i.e. knots are real up to some sufficiently far $R_0 \gg R_a$, where the multipole coupling can be neglected, and complex with geometrically increasing distances until the point where all outgoing waves are effectively damped by ECS to the numerical zero. Now assume that approximately N_0 leading B-splines fit into the inner radius R_a . This will be the “inner basis”. All further B-splines are considered the “outer” basis. There is $N_1 = N - N_0$ outer B-splines. The overlapping B-splines offer a simple means of enforcing the continuity between the inner and outer regions.

By projecting Eq. (7) on the product $B_i(r_1)B_j(r_2)$ and the one-dimensional equations (10) and (13) on $B_i(r_1)$ and $B_j(r_2)$, respectively, we obtain a triplet of matrix equations in the full B-spline basis,

$$\sum_{\ell'_1\ell'_2} \sum_{k,l=1}^N \mathcal{A}_{\ell_1\ell_2\ell'_1\ell'_2,ijkl}^L \psi_{sc,\ell'_1\ell'_2,kl}^{LMS} = \chi_{\ell_1\ell_2,ij}, \quad (17)$$

$$\sum_{\ell'_1\ell'_2} \sum_{m=1}^{N_c^{(1)}} \sum_{k=1}^N \mathcal{B}_{\ell_1\ell_2\ell'_1\ell'_2,mn,kl}^{(1)} F_{m\ell'_1,k}^{(1;\ell'_1,\ell'_2)} = \xi_{n\ell_2,l}^{(1;\ell_1,\ell_2)}, \quad (18)$$

$$\sum_{\ell'_1\ell'_2} \sum_{n=1}^{N_c^{(2)}} \sum_{l=1}^N \mathcal{B}_{\ell_1\ell_2\ell'_1\ell'_2,mn,kl}^{(2)} F_{n\ell'_2,l}^{(2;\ell'_1,\ell'_2)} = \xi_{m\ell_1,k}^{(2;\ell_1,\ell_2)}. \quad (19)$$

Typically, the solution vector $\psi_{sc,\ell'_1\ell'_2,kl}^{LMS}$ is found by a straightforward solution of the coupled set (17). However, the three sets (17)–(19) can be combined into a single system that is mostly much smaller than (17) alone when the assumption (9) is used. The

B-spline equivalents of (9) are

$$\psi_{sc,\ell_1\ell_2,kl}^{LMS} = \sum_{m=1}^{N_c^{(1)}} F_{m\ell_1,k}^{(1)} P_{m\ell_2,l} \quad [k \gtrsim N_0], \quad (20)$$

$$= \sum_{n=1}^{N_c^{(2)}} P_{n\ell_1,k} F_{n\ell_2,l}^{(2)} \quad [l \gtrsim N_0], \quad (21)$$

$$= 0 \quad [k, l \gtrsim N_0].$$

These relations have a simple inversion originating in orthogonality $\sum_{i,j=1}^{N_0} P_{m\ell_1,i} S_{ij} P_{n\ell_2,j} = \delta_{mn}$ of the hydrogen orbitals:

$$F_{m\ell_1,k}^{(1)} = \sum_{i,j=1}^{N_0} P_{m\ell_2,i} S_{ij} \psi_{sc,\ell_1\ell_2,kj}^{LMS} \quad [k \gtrsim N_0], \quad (22)$$

$$F_{n\ell_2,l}^{(2)} = \sum_{i,j=1}^{N_0} P_{n\ell_1,j} S_{ij} \psi_{sc,\ell_1\ell_2,il}^{LMS} \quad [l \gtrsim N_0]. \quad (23)$$

The summation can be truncated already at N_0 due to exponential decay of the orbitals. The matrix S_{ij} is the overlap matrix of the B-spline basis, $S_{ij} = \int B_i(r)B_j(r)dr$.

Having these relations between the full and asymptotic solutions we can now choose the following subset from Eqs. (17)–(19), where we suppressed the angular summations and indices:

$\forall i, j = 1, \dots, N_0 :$

$$\begin{aligned} \chi_{ij} = & \sum_{k,l=1}^{N_0} \mathcal{A}_{ijkl} \psi_{kl} + \sum_{k=N_0+1}^{N_0+O} \sum_{l=1}^{N_0} \sum_{m=1}^{N_c^{(1)}} \mathcal{A}_{ijkl} F_{mk}^{(1)} P_{ml} \\ & + \sum_{k=1}^{N_0} \sum_{l=N_0+1}^{N_0+O} \sum_{n=1}^{N_c^{(2)}} \mathcal{A}_{ijkl} P_{nl} F_{nl}^{(2)}, \end{aligned} \quad (24)$$

$\forall l = N_0 + 1, \dots, N \quad \forall n = 1, \dots, N_c^{(1)} :$

$$\begin{aligned} \xi_{nl}^{(1)} = & \sum_{m=1}^{N_c^{(1)}} \sum_{k=N_0+1}^N \mathcal{B}_{mnlk}^{(1)} F_{mk}^{(1)} \\ & + \sum_{m=1}^{N_c^{(1)}} \sum_{k=N_0+1-O}^{N_0} \mathcal{B}_{mnlk}^{(1)} \sum_{i,j=1}^{N_0} P_{ni} S_{ij} \psi_{kj}, \end{aligned} \quad (25)$$

$\forall k = N_0 + 1, \dots, N \quad \forall m = 1, \dots, N_c^{(2)} :$

$$\begin{aligned} \xi_{mk}^{(2)} = & \sum_{n=1}^{N_c^{(2)}} \sum_{l=N_0+1}^N \mathcal{B}_{mnlk}^{(2)} F_{nl}^{(2)} \\ & + \sum_{n=1}^{N_c^{(2)}} \sum_{l=N_0+1-O}^{N_0} \mathcal{B}_{mnlk}^{(2)} \sum_{i,j=1}^{N_0} P_{mj} S_{ij} \psi_{il}. \end{aligned} \quad (26)$$

These three sub-systems relate the combined solution vector $(\psi_{kl}, F_{mk}^{(1)}, F_{nl}^{(2)})$, see Fig. 2, to the combined right-hand side $(\chi_{ij}, \xi_{nl}^{(1)}, \xi_{mk}^{(2)})$.

If no outer problem is to be solved ($N_0 > 0, N_1 = 0$), Eqs. (24)–(26) reduce to (17) and the symmetrical matrix of the linear equations has the structure illustrated in Fig. 3. The rank of the matrix grows as $O(N^2)$.

When the problem is split into the inner and outer part, the combined matrix has a slightly more complicated structure shown in Fig. 4, but the rank of the combined matrix for fixed inner basis (fixed N_0) scales with $O(N_1) \sim O(N)$ as $N_1 \rightarrow +\infty$, which is already a great improvement over the original $O(N^2)$. Even more, for general M -electron problem, the number of inner solution

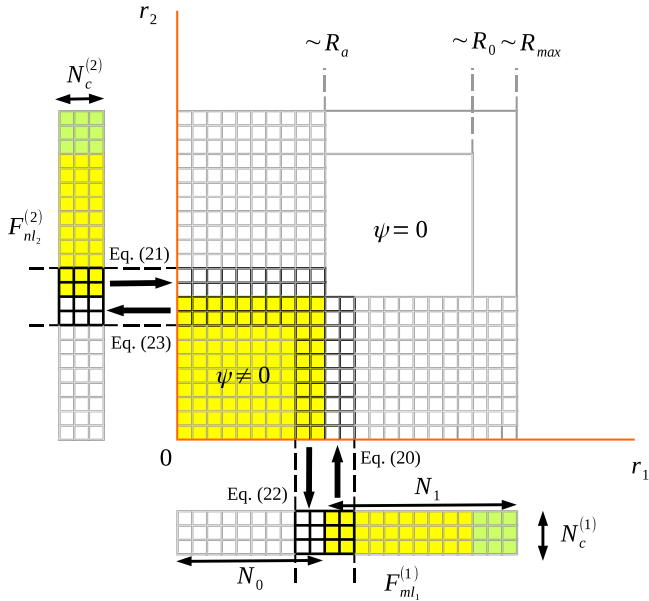


Fig. 2. Relation of the solution parts ψ , $F^{(1)}$ and $F^{(2)}$. Every square corresponds to a B-spline projection of the functions. Only the coloured parts are solved for; yellow elements correspond to real radial B-splines, green to complex B-splines. Elements outside of the inner (outer) B-spline basis are combined from the outer (inner) solutions along the arrows; see also the indicated equations. (For interpretation of the references to colour in this figure legend, the reader is referred to the web version of this article.)

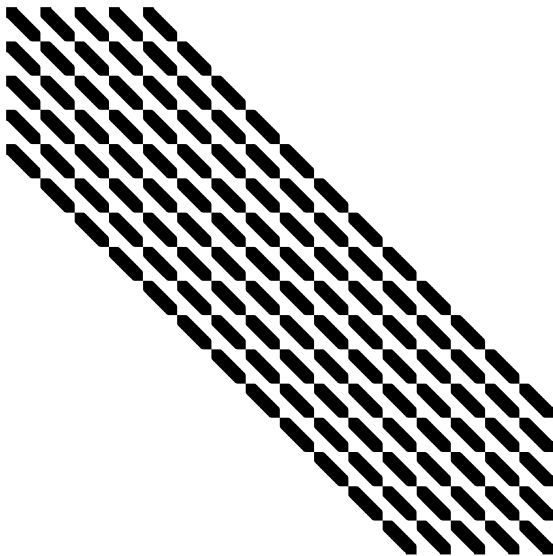


Fig. 3. Structure of the original B-spline matrix A of Eq. (7) or (17) (one angular block). The matrix corresponds to the two-dimensional nature of the problem—it has a regular structure of a tensor product of one-dimensional banded matrices.

elements grows as $O(N_0^M)$, but with the new approach still just a few *one-dimensional* (hence $O(N^1)$) channels will dominate as $N \rightarrow +\infty$.

In the Hex implementation of the ECS/B-spline method the full system (7) is solved iteratively using the *conjugate orthogonal conjugate gradients* (COCG) algorithm, preconditioned by inversion of the diagonal blocks. The inversion is done iteratively, again, with a user-selectable preconditioner. As noted, matrix blocks with non-zero number of asymptotic channels (Fig. 4) do not possess the regular nested structure of the original inner-only problem (Fig. 3),

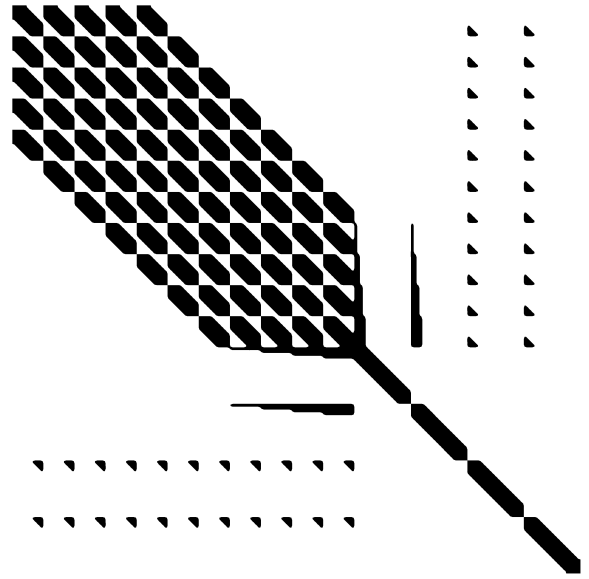


Fig. 4. Structure of the combined set of Eqs. (24)–(26). The inner problem (top left) keeps the two-dimensional tensor-product nature, whereas the outer problems for the various channels (right bottom) are one-dimensional. The inner and outer problems are coupled (left bottom and right top). Generally the one-dimensional diagonal blocks can be also coupled to each other, but always only within a set corresponding to $F_{n\ell}(r_1)$ or $F_{n\ell}(r_2)$, whenever dipole or higher coupling is possible, see (10) and (13). This figure, however, corresponds to the matrix \mathcal{A}_{0000}^0 dealing with $L = \ell_1 = \ell_2 = 0$ solution blocks; these solutions asymptotically converge to a sum of s -states which are not coupled by any multipole.

so that it is not easily possible to use the effective Kronecker product approximation preconditioner [15,16]. However, the matrices are relatively small and it is still computationally feasible to use the sparse incomplete LU factorization as a preconditioner for the inner iterations.

3. Results

To illustrate the benefits of the suggested approach we did several simple calculations of the electron-hydrogen scattering at energies right above two chosen excitation thresholds. All calculations are for transitions between the s -states and for total quantum numbers $L = S = \mathcal{M} = 0$, $\ell_{1,2} \geq 0$. The B-spline knot spacing is $1 a_0$ in the real part and gradually increasing in the complex part, which is $500 a_0$ long. The results and the required computation times are summarized in Tables 1 and 2. The scattering equations have been solved both by the original method presented in [8] (upper half of each table) and by the new method with dividing radius R_a (lower half). The upper half of each table documents an undesired rapid increase of the solution time with the increasing real grid length R_0 , while the radial convergence of the cross sections is quite slow. The lower half of each table contains the split calculation with the inner region radius R_a chosen far enough to contain all asymptotically forbidden components of the solution. Clearly, the channel reduction introduced in the previous section dramatically speeds up the calculation while maintaining the accuracy, and allows an extension of the real radial grid to large distances. The calculations have been run on a 4-core Intel i7-4790K processor with the MUMPS LU decomposition library [17] in an out-of-core mode used for preconditioning. Of course, the speed-up of the new method does not depend on a particular choice of the numerical library and was observed also for other packages supported by the code (e.g. Pardiso, UMFPACK, SuperLU).

We also present three real-world sample results for excitations of the hydrogen atom from the ground state to the 3s, 3p and

Table 1

Partial singlet cross sections for the $H(1s) \rightarrow H(2s)$ transition at projectile impact energy $E_i = 0.755$ Ry. The angular states up to $0 \leq \ell_{1,2} \leq 3$ have been included. The total energy is $E_{\text{tot}} = -0.245$ Ry, which is 0.005 Ry above the $n = 2$ threshold, with 2 allowed asymptotic channels: 1s and 2s. Using $R_a = 100 a_0$ as the inner region's radius in the inner-outer-region calculation is enough to match the inner-region-only results within 0.1%.

$R_a [a_0]$	$R_0 [a_0]$	$\sigma_0 [a_0^2]$	Time [min]
–	200	0.1135	1.0
–	400	0.1151	3.5
–	800	0.1147	39.5
–	1600	0.1145	337
100	200	0.1135	0.1
100	400	0.1151	0.1
100	800	0.1147	0.1
100	1600	0.1146	0.1

Table 2

Partial singlet cross sections for the $H(2s) \rightarrow H(3s)$ transition at projectile impact energy $E_i = 0.14$ Ry. The angular states up to $0 \leq \ell_{1,2} \leq 7$ have been included. The total energy is $E_{\text{tot}} = -0.11$ Ry, which is approximately 0.001 Ry above the $n = 3$ threshold, with 3 allowed asymptotic channels: 1s, 2s and 3s. Using $R_a = 200 a_0$ as the inner region's radius in the inner-outer-region calculation is enough to match the inner-region-only results within 0.1%.

$R_a [a_0]$	$R_0 [a_0]$	$\sigma_0 [a_0^2]$	Time [min]
–	400	0.1061	101
–	800	0.1597	533
–	1 600	0.2078	1094
200	400	0.1062	2.7
200	800	0.1598	2.7
200	1 600	0.2079	2.7
200	6 400	0.2406	2.7
200	64 000	0.2506	3.9
200	640 000	0.2516	72.6

3d states compared to previously published data in Fig. 5. These transitions have been chosen due to the availability of reference data. We intend, however, to use the new extension particularly for calculations of scattering on excited states, where the long-range potentials play a more important role, and to publish the complete datasets in a separate paper.

4. Conclusion

In this paper we have presented a method that considerably reduces the computational requirements of the low-energy electron-atom scattering calculations by splitting the full problem into the inner and outer problems, similarly to the R -matrix approach. But unlike in the R -matrix method the diagonalization of the large inner many-electron hamiltonian is avoided. The inner and outer problems are solved in a common radial B-spline basis and they are coupled through the overlapping B-splines. The boundary condition is replaced by the ECS complex damping region.

The new formulation allows to extend the full radial basis to large distances to account for any long-range potentials. We intend to use the new method to finish the Hex database [19], which is planned to contain a superset of electron-hydrogen scattering data currently available in other online databases (e.g. Aladdin or NIST) with focus on applications in stellar physics.

Acknowledgements

The study was supported by the Charles University in Prague, project GA UK No. 730214, and by the project SVV-260320.

Computational resources were provided by the CESNET LM2015042 and the CERIT Scientific Cloud LM2015085, provided under the programme “Projects of Large Research, Development, and Innovations Infrastructures”.

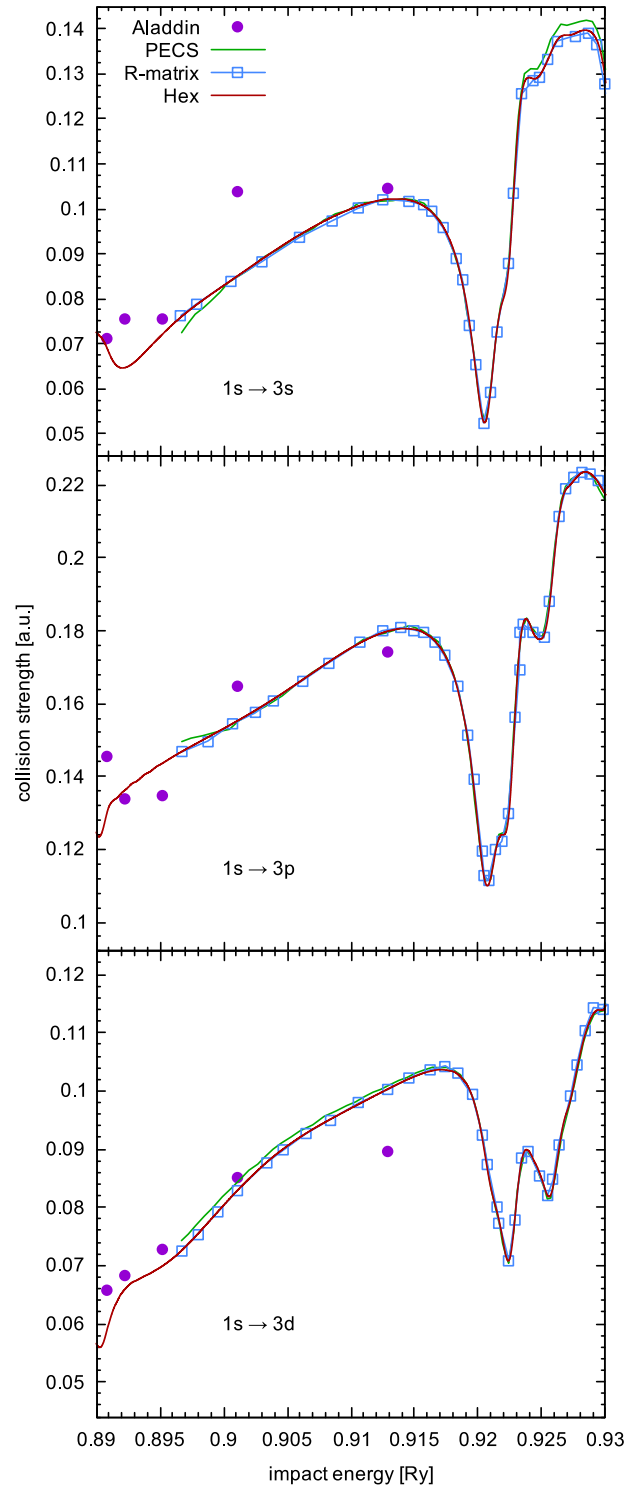


Fig. 5. Radially converged cross sections for transitions $H(1s) \rightarrow H(3s)$, $H(3p)$ and $H(3d)$, multiplied by the impact energy. The present calculation is labelled “Hex”. The reference data are taken from the Aladdin database [18], and from the paper [11] (both the curves “PECS” and “ R -matrix”; the latter called “ R -matrix Propagator” in the original paper). The new results are very close to the PECS data, but even closer to the R -matrix results, which is an expected behaviour due to the long-distance reach of the new method.

This work was supported by The Ministry of Education, Youth and Sports from the Large Infrastructures for Research, Experimental Development and Innovations project “IT4Innovations National Supercomputing Center LM2015070”.

References

- [1] O. Zatsarinny, K. Bartschat, *J. Phys. B: At. Mol. Opt. Phys.* 46 (2013) 112001.
- [2] I. Bray, et al., *J. Phys. B: At. Mol. Opt. Phys.* 35 (2002) R117.
- [3] I. Bray, et al., *Phys. Rep.* 520 (2012) 135–174.
- [4] T.N. Rescigno, C.W. McCurdy, *Phys. Rev. A* 62 (2000) 032706.
- [5] C.W. McCurdy, M. Baertschy, T.N. Rescigno, *J. Phys. B: At. Mol. Opt. Phys.* 37 (2004) R137.
- [6] P.L. Bartlett, *J. Phys. B: At. Mol. Opt. Phys.* 39 (2006) R379.
- [7] M.V. Volkov, et al., *Phys. Rev. A* 83 (2011) 032722.
- [8] J. Benda, K. Houfek, *Comput. Phys. Comm.* 185 (2014) 2903–2912.
- [9] C.W. McCurdy, F. Martín, *J. Phys. B: At. Mol. Opt. Phys.* 37 (2004) 917.
- [10] T.F. O'Malley, L. Spruch, L. Rosenberg, *J. Math. Phys.* 2 (1961) 491.
- [11] P.L. Bartlett, et al., *Phys. Rev. A* 74 (2006) 022714.
- [12] S.B. Zhang, J.G. Wang, R.K. Janev, *Phys. Rev. A* 81 (2010) 032707.
- [13] K. Bartschat, *Computational Atomic Physics*, Springer-Verlag, 1996.
- [14] C. de Boor, *A Practical Guide to Splines*, Springer, New York, 1978.
- [15] J. Benda, K. Houfek, *Comput. Phys. Comm.* 204 (2016) 216–217. <https://sourceforge.net/projects/hecs>.
- [16] Bar-On, et al., *Appl. Numer. Math.* 33 (2000) 95–104.
- [17] P.R. Amestoy, I.S. Duff, J. Koster, J.-Y. L'Excellent, *SIAM J. Matrix Anal. Appl.* 23 (2001) 15–41.
- [18] I. Bray, A.T. Stelbovics, *Adv. At. Mol. Opt. Phys.* 35 (1995) 209–254. <https://www-amdis.iaea.org/ALADDIN/>.
- [19] J. Benda, K. Houfek, *Comput. Phys. Comm.* 185 (2014) 2893–2902. <http://utf.mff.cuni.cz/data/hex>.